# Elevating the Concentration of Na ions to 1 in P2 Type Layered Oxide Cathodes

Hari Narayanan Vasavan <sup>a \*</sup>, Samriddhi Saxena <sup>a</sup>, Velaga Srihari <sup>b</sup>, Asish Kumar Das <sup>a</sup>,

Pratiksha Gami <sup>a</sup>, Neha Dagar <sup>a</sup>, Sonia Deswal <sup>c</sup>, Pradeep Kumar <sup>c</sup>, Himanshu Kumar

Poswal <sup>b</sup>, and Sunil Kumar <sup>a \*\*</sup>

<sup>a</sup> Department of Metallurgical Engineering and Materials Science, Indian Institute of Technology Indore, Simrol, 453552, India.

<sup>b</sup> High Pressure & Synchrotron Radiation Physics Division, Bhabha Atomic Research Centre, 400085 Mumbai, India

<sup>c</sup> School of Physical Sciences, Indian Institute of Technology Mandi, Himachal Pradesh, 175005, India

\* Corresponding Author: mtphd2206105002@iiti.ac.in

\*\* Corresponding Author: sunil@iiti.ac.in

**Abstract** 

Layered oxide cathodes, particularly those with P2 and P3 type structures, have lower specific

capacities limited by the Na-ion content in their structure. In this study, we have elevated the

Na content to its uppermost limit with a NaMn $\frac{4.5}{8}$ Al<sub>1</sub>Ni $\frac{2.5}{8}$ O<sub>2</sub> cathode. The material was

synthesized in a monophasic P3, monophasic P2 (with a minor O3 phase), and biphasic P3/P2

configuration. During electrochemical testing, the biphasic P3/P2 and the monophasic P2 type

compounds exhibited excellent performance, with specific capacities reaching 102 mAh g-1

and 87 mAh g<sup>-1</sup>, respectively, at 6C. A full cell fabricated using the monophasic P2 type

cathode demonstrated a specific capacity of 123 mAh g<sup>-1</sup> at 0.1C and retained 90% of its initial

specific capacity after 200 cycles at 0.2C. The structural integrity of both the biphasic P3/P2

and the monophasic P2 type cathode materials was supported by the operando synchrotron

XRD data, which showed no phase transformations and P2 phase showing only a 0.78%

variation in unit cell volume. These findings highlight the transformative potential of achieving

high Na-ion concentrations in P2-type cathode materials, paving the way for developing high-

performance sodium-ion batteries.

**KEYWORDS**: Electrochemistry; Layered compounds; Sodium; *Operando* Synchrotron XRD;

### Introduction

Developing sustainable and high-performance energy storage systems is paramount in addressing the increasing global energy demand and environmental challenges.<sup>[1-2]</sup> Owing to the abundance and low cost of sodium resources, sodium-ion batteries (NIBs) have gained significant attention as a viable alternative to lithium-ion-based energy storage systems.<sup>[3-7]</sup> However, the advancement of NIBs heavily relies on developing efficient cathode materials. Various cathode materials have been explored for NIBs, including layered oxides, NASICON-type, and Prussian blue analogs. NASICON (Na Super Ionic Conductor) type materials are known for their structural stability, making them promising candidates for NIB cathodes. Similarly, Prussian blue analog cathodes offer open frameworks that facilitate rapid sodium ion diffusion, contributing to their high-rate capabilities. Despite these advantages, challenges such as limited capacity and stability issues under prolonged cycling still need to be addressed.<sup>[7-10]</sup>

Layered oxide cathodes (represented by the formula  $Na_xTMO_2$ ;  $0 < x \le 1$ ; TM- transition metal cations), particularly those with P2 and P3 type structures, have shown great promise due to their high theoretical capacities and favorable electrochemical characteristics. P2 and P3 type structures are characterized by their prismatic sodium sites, which provide a relatively stable and open structure that facilitates high sodium diffusion, leading to good rate performance and cycling stability. [11-17] Over the years, biphasic cathode materials involving P3/P2 type structures have also emerged as leading contenders for potential applications in NIBs [18-25]. Despite their potential, these materials have been constrained by their maximum Na ion content, limiting their specific capacity. P2-type structures are typically considered to hold up to only x = 0.8 Na ions in their structures, the notable exception being Na<sub>0.85</sub>Li<sub>0.08</sub>Ni<sub>0.30</sub>Mn<sub>0.62</sub>O<sub>2</sub> prepared by Zhao et al.. [26] When synthesized with higher sodium ion content, the O3-type structure tends to appear alongside the P-type structure, increasing in proportion as the sodium

content rises, ultimately resulting in a pure O3 phase in NaTMO<sub>2</sub> compounds.<sup>[27-28]</sup> O3-type structures, characterized by their octahedral sodium sites, are often prone to structural degradation and phase transitions during cycling, limiting their long-term performance.<sup>[22, 28-34]</sup>

In an effort to identify the optimal cathode material, we previously examined the structural and electrochemical performance of various compositions in the Na<sub>3/4</sub>(Mn-Al-Ni)O<sub>2</sub> pseudoternary system.<sup>[18-21]</sup> These compositions were mainly prepared in 3 different phases: monophasic P3, monophasic P2 (with a minor O3 phase), and a biphasic P3/P2. As a result, the biphasic P2/P3-type  $Na_{\frac{3}{4}}Mn_{\frac{4.5}{8}}Al_{\frac{1}{8}}Ni_{\frac{2.5}{8}}O_2$  material was identified as the optimal cathode, showcasing impressive rate performance and cyclic stability. Additionally, our studies revealed that the presence of Al<sup>3+</sup> in the P3 type structure helped prevent P3 to O3 type transitions, which were observed in non-Al-containing materials in the pseudo-ternary system, such as the P3 type  $Na_{\frac{3}{4}}Mn_{\frac{3}{4}}Ni_{\frac{1}{4}}O_{2}$ . [18, 20] It was concluded that  $Al^{3+}$  could stabilize the P3-type structure during the discharge cycle even when Na concentrations reached values beyond 0.8. There have also been recent reports of P3-type LO cathodes synthesized with x = 1 Na ions [35]. Since P2-type LOs are considered an ordered form of P3-type compounds with 2 distinct Na sites, we have tried to leverage the phase stabilizing property of Al<sup>3+</sup> to prepare high Na-containing P2-type cathodes by increasing the concentration of Na in  $Na_{\frac{3}{4}}Mn_{\frac{4.5}{8}}Al_{\frac{1}{8}}Ni_{\frac{2.5}{8}}O_2$  to  $NaMn_{\frac{4.5}{8}}Al_{\frac{1}{8}}Ni_{\frac{2.5}{8}}O_{2}$ . It was found that the presence of  $Al^{3+}$  can also prevent the formation of O3-type phases in high Na-containing P3 and P2-type layered oxide cathodes. Moreover, even with an increased Na-content in P2-type NaMn $_{\frac{4.5}{8}}$ Al $_{\frac{1}{8}}$ Ni $_{\frac{2.5}{8}}$ O $_{2}$  demonstrated impressive rate performance and cyclic stability.

#### **Materials and Methods**

The cathode samples were synthesized through a conventional sol-gel method. Aluminum nitrate nonahydrate, nickel acetate tetrahydrate, manganese (II) acetate tetrahydrate, and sodium nitrate were precursors. After dissolving the precursors in deionized water, appropriate amounts of ethylene glycol and citric acid were added to the solution, which was then heated to produce a gel. This was then dried and calcined at varying temperatures (650 – 850 °C) for 8 h to obtain the final products.

Inductively coupled plasma atomic emission spectrometry (ICP-AES) (SPECTRO Analytical Instruments GmbH, Germany, Model: ARCOS, Simultaneous ICP Spectrometer) was used to determine the specific chemical compositions of the cathode materials. Structural parameters of the materials were studied using X-ray diffraction (XRD) data, recorded with the help of a Malvern PanAnalytical Empyrean diffractometer (Cu-Kα radiation source) at room temperature. Rietveld refinement of XRD data was carried out using the *TOPAS Academic* (version 6) software package.<sup>[36]</sup> A JEOL field emission scanning electron microscope (FESEM) (model JEOL-7610) was used to obtain the SEM micrographs. The X-ray photoelectron spectra (XPS) were recorded using a Thermo Fisher Scientific - Naxsa base equipped with an Al Kα X-ray source (1486.6 eV). *Operando* Synchrotron XRD measurements were taken at the extreme conditions angle dispersive/energy dispersive synchrotron X-ray diffraction beamline (BL11) at Indus-2 (RRCAT) with a beam wavelength of 0.74 Å.

The electrochemical tests were conducted using half-cells containing an electrolyte of 1M NaClO<sub>4</sub> in a 1:1 volume ratio of ethylene carbonate to propylene carbonate and a Whatman GF/D filter paper separator. These cells were evaluated on a Neware battery tester (CT-4008T). The cathode samples were fabricated by blending 75 wt.% active material, 10 wt.% Ketjen black, and 15 wt.% PVDF to create a slurry, which was cast onto an aluminum current collector.

The mass loading of the samples was approximately  $\sim$  4-5 mg cm<sup>-2</sup>, and the C-rates were determined based on a nominal capacity of 150 mAh g<sup>-1</sup>. In a similar process, the negative electrode was formed by mixing commercially available hard carbon with Ketjen black and PVDF binder in NMP, using the same 75:10:15 weight ratio. This was then coated onto an Al foil and dried. The hard carbon (HC) was then used to make HC half cells and cycled at 0.1C thrice between 0.01 V and 2.5 V before being used as the anode material in full cells. The optimum N/P ratio for the full cells was around 1.06. The galvanostatic intermittent titration technique (GITT) was carried out using a Neware battery tester (CT-4008T). The technique involves applying a constant current pulse for 10 minutes, followed by a dwell time of 30 minutes, during which the cell is allowed to reach a quasi-equilibrium state. The mass loading for the samples was  $\sim$  4-5 mg cm<sup>-2</sup>, and C-rates were calculated, taking the nominal capacity of 150 mAh g<sup>-1</sup> (assuming a Na<sup>+</sup> extraction of 0.60). An NF Corp LCR meter (model: ZM 2376) was used to obtain the impedance data in the 1 Hz  $\sim$  1 MHz frequency range at room temperature. The Impedance data was obtained for all samples at 2.5 V.

### **Results and Discussion**

This work and the composition Na1 is an extension of an earlier study exploring the Na<sub>3</sub>/4(Mn-Al-Ni)O<sub>2</sub> pseudo-ternary system, in which the composition Na<sub>3</sub>/4 Mn<sub>4.5</sub>Al<sub>1</sub>Ni<sub>2.5</sub>O<sub>2</sub> was identified as the optimal cathode material. Na1 was prepared in 3 configurations: monophasic P3 (Na1-P3), monophasic P2 (with a minor O3 phase, henceforth referred to as Na1-P2), and biphasic P3/P2 (Na1-P3P2) with almost equal proportions of P3 and P2. This was achieved by calcinating the samples at different temperatures. This yielded a P3 phase at lower temperatures (650 °C) with increasing P2 phase fractions as the calcination temperature increased. The composition of Na1-P3, Na1-P2, and Na1-P3P2 was analyzed using ICP-AES (Table S1), which confirmed the concentration of Na to be close to 1.0 in all three materials. The crystal structure and phase configurations of the three materials were studied using Rietveld

refinement of XRD data displayed in Figure 1. The diffraction peaks in Na1-P3 calcined at 650 °C were indexed with the *R3m* space group, while that of Na1-P2 calcinated at 850 °C was indexed using the *P6*3/*mmc* space group. The analysis also confirmed the equal proportions of the P3 and P2 phases in the Na1-P3P2 sample, which was calcined at 800 °C for 8 h. Additionally, the presence of a minor O3 phase was also identified in both Na1-P3P2 and Na1-P2. This was expected as P2-type phases are rarely reported to contain Na concentrations beyond 0.8.

Ordinarily, an O3-type phase is expected in high Na-containing layered oxide materials. Instead, in Na1, a P3 phase formed at a lower calcination temperature and converted into a P2type phase at higher calcination temperatures, with O3 crystalizing only as a minor phase. This could be due to the presence of Al<sup>3+</sup> in the material, which may favor the formation of P-type phases. This was also noticed in our previous works involving the Na<sub>3/4</sub>(Mn-Al-Ni)O<sub>2</sub> pseudo ternary system where operando synchrotron XRD on the P3 type materials showed that the P3 to O3 type transformations observed in a non-Al containing material was found to be absent in all Al substituted samples even after being discharged up to 1.5 V (where Na concentrations reach close to 1.0).[18-20] The conclusion drawn from that study was that the presence of Al<sup>3+</sup> in layered oxide compounds can stabilize the P3 crystal structure enough to prevent the 'slab gliding' mechanism that transforms it into an O3-type phase when Na ions are inserted into the structure electrochemically during cycling. The fact that the P-type phases contributed to most of the phase composition in the Na1 cathode material during synthesis proves that the Al3+ favors the formations of the P-type materials. This could be due to stronger Al-O bonds in the transition metal (TM) layers (501.9 kJ mol<sup>-1</sup>) compared to Mn–O bonds (362 kJ mol<sup>-1</sup>). These stronger bonds broaden the Na interlayer spacing, increasing the volume of the Na-O6 prismatic sites within the LO structure while simultaneously reducing the interlayer spacing between TM-O<sub>2</sub> layers (Figure S1) [37]. The expansion of the Na-O layers caused by the

presence of Al ions enables the compounds to create more favorable sites for sodium ion intercalation, facilitating the incorporation of a higher number of Na ions within the P2 unit cell when calcinated at a higher temperature.

The crystallographic parameters of all these materials obtained after Rietveld refinement are summarised in Table 1. Interestingly, the P2 unit cell volume was found to be  $80.17 \, \text{Å}^3$ , which was lower than the previously reported volume of the P2 type  $\text{Na}_{\frac{3}{4}}\text{Mn}_{\frac{4.5}{8}}\text{Al}_{\frac{1}{8}}\text{Ni}_{\frac{2.5}{8}}\text{O}_2$  due to the former's lower c parameter. [18] This resulted from shrinking Na-O6 prisms in the Na1-P2 type structure, which could hinder the diffusion of Na-ions through the material initially during charging. However, unit cell parameters of the P3 structure remained unaffected by the increase in Na-ion concentration and were found to be similar to those of the P3 type  $\text{Na}_{\frac{3}{4}}\text{Mn}_{\frac{4.5}{8}}\text{Al}_{\frac{1}{8}}\text{Ni}_{\frac{2.5}{8}}\text{O}_{2}$ .

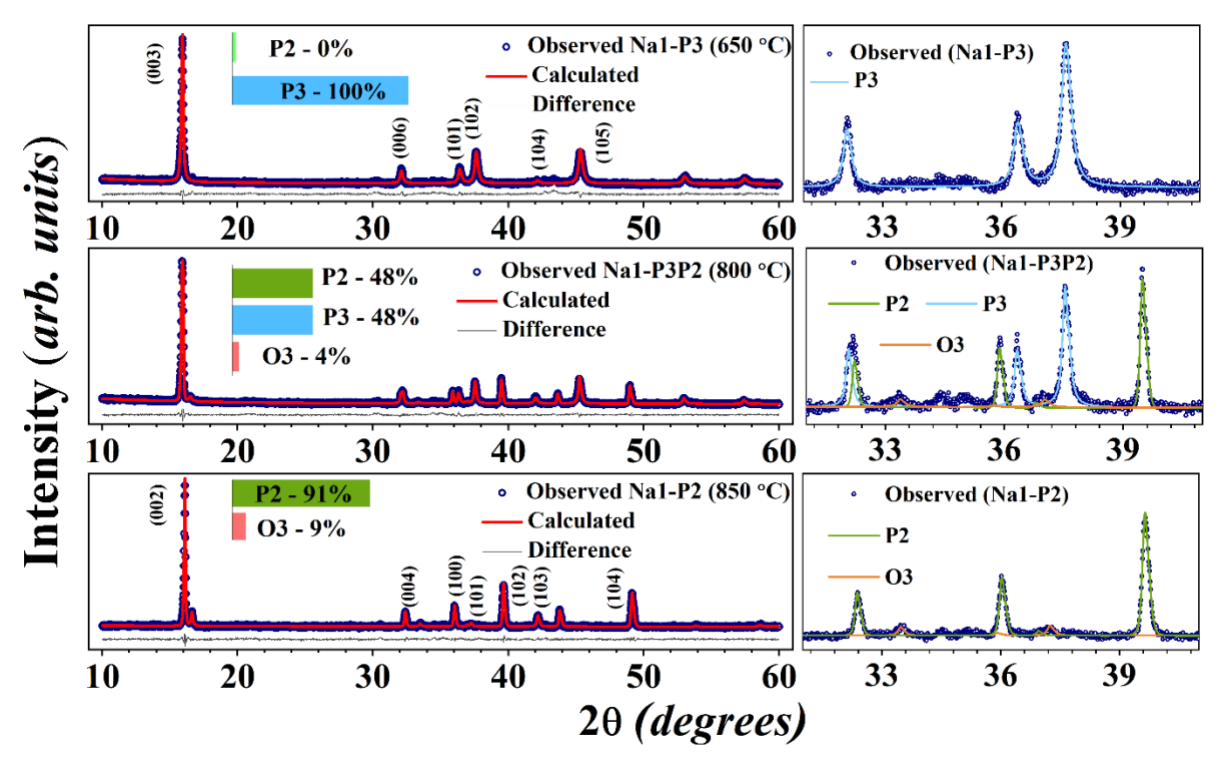


Figure 1. Rietveld refinement of XRD data for Na1-P3, Na1-P3P2, and Na1-P2 materials with enlarged views of their respective deconvoluted P2, P3, and O3 phases in the vicinity of 30-40° 2θ range.

**Table 1.** Lattice parameters of Na1-*x* samples obtained from the Rietveld refinement of room temperature XRD data.

Sample	Phase (Fraction)	a (Å)	c (Å)	V (Å <sup>3</sup> )	Reliability Factors
Na1-P3	P3 (100%)	2.8857 (5)	16.7656 (2)	121.05 (4)	R <sub>exp</sub> : 2.93 R <sub>wp</sub> : 4.51 GOF: 1.54
Na1-P3P2	P3 (48%)	2.8869 (3)	16.7745 (2)	120.86 (2)	R <sub>exp</sub> : 2.49 R <sub>wp</sub> : 2.99 GOF: 1.20
	P2 (48%)	2.8891 (4)	11.1125 (1)	80.34 (2)	
	O3 (4%)	2.9404 (3)	16.10 (1)	120.58 (3)	
Na1-P2	P2 (91%)	2.8834 (2)	11.1669 (4)	80.404 (5)	R <sub>exp</sub> : 2.01 R <sub>wp</sub> : 2.41 GOF: 1.28
	O3 (9%)	2.9409 (3)	16.097 (2)	120.05 (5)	

The microstructure of the Na1 samples was studied using a field emission secondary electron microscope (FESEM). The SEM micrographs of the materials in Figure 2 show an increasing degree of particle agglomeration in samples synthesized at higher calcination temperatures. Smaller particle sizes and relatively lower degree of agglomeration of particles are preferred in cathode materials as they usually support better ionic conduction. [38-39] Hence, Na1-P2, with its slightly high degree of particle agglomeration, may not fare well in terms of rate performance. The elemental maps of the Na1-P3P2, shown in Figure 2(b1-b5), show a uniform distribution of its constituent elements within the sample.

The oxidation states of the constituent elements in the monophasic P3 and P2 type samples were identified by analyzing their respective Mn 2p and Ni 2p XPS spectra (Figure S2). The Mn 2p XPS spectra could be deconvoluted into 4 peaks at 641.8 & 653.2 eV and 643.2 & 654.7 eV, suggesting a combination of 3+ and 4+ oxidation states for Mn ions in both materials.<sup>[40-42]</sup> In the Ni 2p XPS spectra, the peaks at 854.26 and 871.75 eV indicated that Ni ions existed primarily in a 2+ oxidation state.<sup>[40-42]</sup>

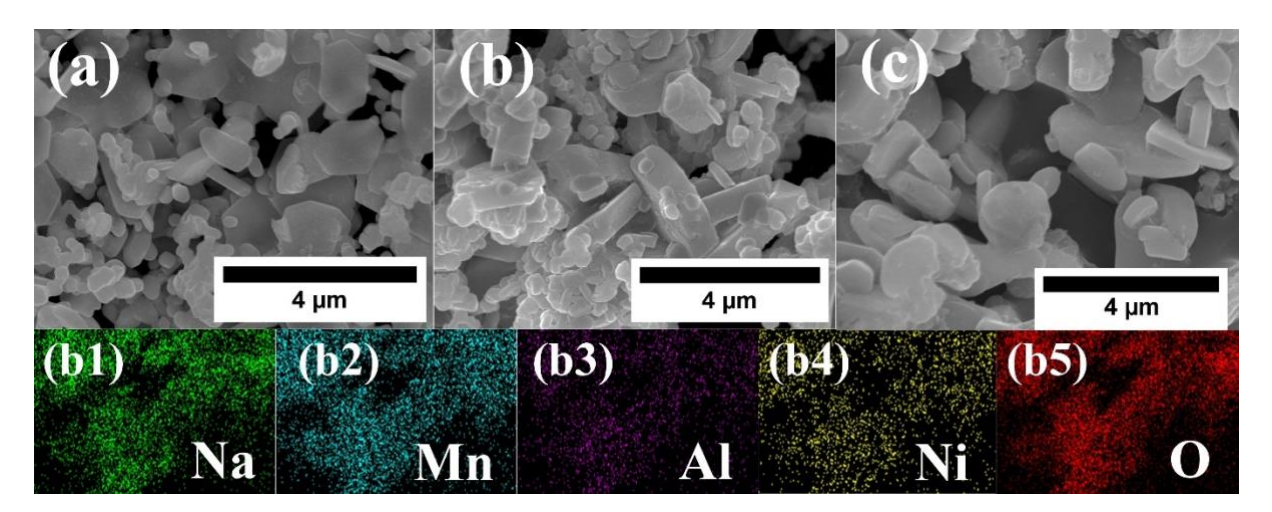


Figure 2. SEM micrographs of (a) Na1-P3, (b) Na1-P3P2, and (c) Na1-P2 samples with (b1-5) representing the maps of different elements in Na1-P3P2.

The electrochemical properties of the three cathode materials were tested in half cells in a voltage range between 1.5 V and 4.0 V. This was to ensure the activation of both Mn<sup>3+/4+</sup> and Ni<sup>2+/4+</sup> redox couples, which are active between 1.5-2.5 V and 3.0-4.0 V, respectively.<sup>[43-46]</sup> Figure S3 and Figure 3 depict the galvanostatic charge-discharge (GCD) curves of Na1-P3, Na1-P2, and Na1-P3P2 at various C rates, along with their respective dQ/dV vs. voltage plots at 0.1C. The curves show that the P3-type material exhibited the highest specific capacity of 196 mAh g<sup>-1</sup> at 0.1C, which decreased progressively in the materials with a higher P2 phase. This discrepancy could be attributed to structural differences between the P3 and P2 phases. The P3 structure permits the extraction of a higher amount of Na ions (0.87) in the 2.0–4.0 V

range, likely by undergoing multiple phase transformations. In contrast, the P2 structure allows for the extraction of only limited Na-ions (0.65) within the same voltage range.

The dQ/dV vs. voltage plots of all 3 materials also confirm the activity of Mn³+/4+ and Ni²+/4+ redox couples. Compared to its P2-type Na³ Mn⁴  $\frac{4.5}{8}$ Al¹ Ni²  $\frac{1.5}{8}$ O2, Na1-P2 showed significant improvement in rate performance, exhibiting specific capacities reaching up to 121 mAh g¹ and 87 mAh g¹ at 1C and 6C, respectively (Figure 4(a)). The subtle differences in peak voltages and the appearance of smaller new peaks in the dQ/dV vs. Voltage curves for both Na1-P3P2 and Na1-P2 compounds can be attributed to their structural differences. In Na1-P3P2, sodium ions are extracted from two distinct phases, P3 and P2, each with different activation energies corresponding to the unique sites occupied by Na-ions. In contrast, Na1-P2 consists of a single P2 phase, which actively facilitates the intercalation and deintercalation of Na ions. Surprisingly, the Na1-P3 showed a significant decline in rate performance compared to the P3 type Na³ Mn⁴ Na1-P3 showed a significant decline in rate performance compared to the P3 type Na³ Mn⁴  $\frac{1.5}{8}$ Al¹ Ni²  $\frac{1.5}{8}$ O2, and could be due to multiple phase transitions from P3 to P3' and P3'' during cycling. [47-48]

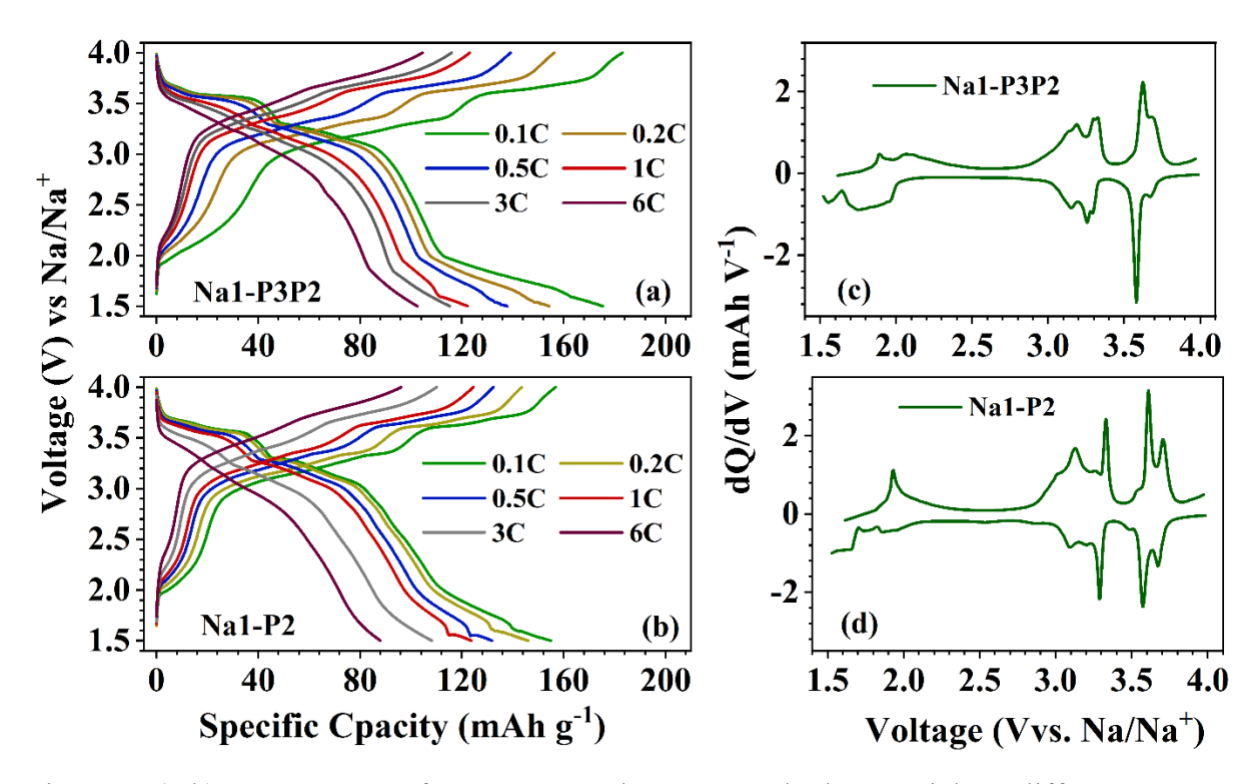


Figure 3. (a-b) GCD curves of Na1-P3P2 and Na1-P2 cathode materials at different C rates with (c-d) showing their respective dQ/dV vs. voltage plots at 0.1C.

In contrast, Na1-P3P2 demonstrated significantly enhanced rate performance compared to its single-phase counterparts, achieving specific capacities close to 102 mAh g<sup>-1</sup> at 6C. This remarkable enhancement in rate performance for the biphasic cathode material can be attributed to the continued existence of high Na-ion conducting P-type phases. Furthermore, the high specific capacities demonstrated by the Na1 series of materials are also achievable in a full cell configuration, as each started from a Na1.0 configuration and did not require the insertion of any additional sodium ions from the Na metal anode during cycling.

Following the rate performance tests, the cyclic stability of the cathode materials was evaluated within a voltage range of 1.5-4.0 V at 1C over 300 cycles (Figure 4(b)). The results indicated that Na1-P2 exhibited the highest cyclic performance with approximately 80% capacity retention, followed by Na1-P3P2 with 73% capacity retention after 300 cycles. Despite having a significantly lower specific capacity at 1C (80 mAh g<sup>-1</sup>), the monophasic P3-type cathode only retained about 66% of its capacity. Additionally, the cyclic curve for the P3-type material

showed a marked increase in slope after about 200 cycles. This is indicative of a rapid capacity decline with each subsequent cycle, which may have been caused by a severe structural degradation in the cathode material. Although subtle, a similar increase in slope was also observed in the biphasic Na1-P3P2 after 250 cycles. This provides two key insights: first, the capacity decline in the biphasic material may also be caused by structural degradation of its P3 phase; second, the presence of the P2 phase in the biphasic cathode is beneficial in both delaying the onset of severe structural degradation in the P3 type structure and reducing its intensity in each subsequent cycle. Furthermore, contrary to what was observed in the other materials in the Na<sub>3/4</sub>(Mn-Al-Ni)O<sub>2</sub> pseudo-ternary system, the biphasic Na1-P3P2, for the first time, has shown inferior cyclic properties compared to its monophasic P2, counterpart.<sup>[18-19]</sup> This points to the excellent structural stability of the high Na-containing P2 structure.

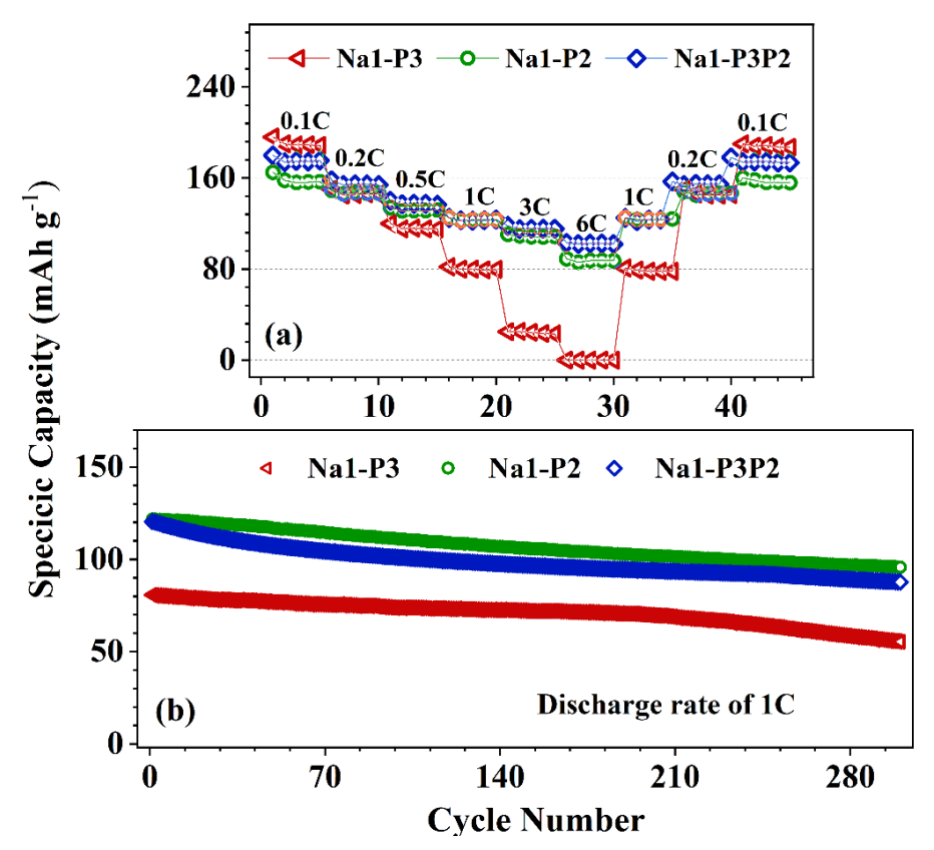


Figure 4. (a) Rate performance of Na1 series of cathodes at various C rates and their (b) cyclic performance curves at 1 C.

The superior cyclic performance of Na1-P2 cells is evident from the Nyquist plots presented in Figure S4. The equivalent circuit analysis of the Nyquist plot revealed that the total resistance (R1 + R2 + R3) of the Na-P2 half-cell decreased from 150  $\Omega$  to 230  $\Omega$  after cycling, while the cycled Na1-P3 cell exhibited a significantly higher total resistance exceeding 700  $\Omega$ . In Na1 P3, both R2 (solid electrolyte interface resistance) and R3 (charge transfer resistance) show significantly high values ('~300  $\Omega$  and ~370  $\Omega$ , respectively) after 300 cycles compared to Na1P3P2 and Na-P2, which could be attributed to structural degradation and particle cracking within the material. Furthermore, results from the GITT experiments (Figure S5) demonstrated that both Na1-P2P3 and Na1-P2 cells achieved the highest diffusion coefficients, approximately  $4 \times 10^{-10}$  cm<sup>2</sup> s<sup>-1</sup>, nearly four times higher than that of the Na1-P3 sample.

After cyclic tests on the Na1-P2 half cells, the electrochemical performance of the Na1-P2 cathodes was evaluated in a full-cell configuration. In this setup, a pre-sodiated hard carbon was used as the anode (the GCD curve of HC half cells is displayed in Figure S6). Figure 5(a) presents the GCD curves of the Na1-P2 full cells between 1.5 to 4.0 V at various C rates. At a discharge rate of 0.1C, the Na1.0-P2 full cell exhibited a specific capacity of 123 mAh g<sup>-1</sup>. The lower capacity observed in the full cell, compared to the Na1-P2 half-cell, is attributed to the limited activity of the Mn<sup>3+/4+</sup> redox couples in the cathode, which may only be active at further lower voltages in the full-cell configuration. The Na1-P2 full cells demonstrated excellent cyclic performance, retaining approximately 90% of their initial capacity after 200 cycles at a charge-discharge rate of 0.2 C (Figure 5(b)). This impressive cycle stability might also be due to the limited activity of Mn<sup>3+/4+</sup> redox couples within the cycled voltage window.

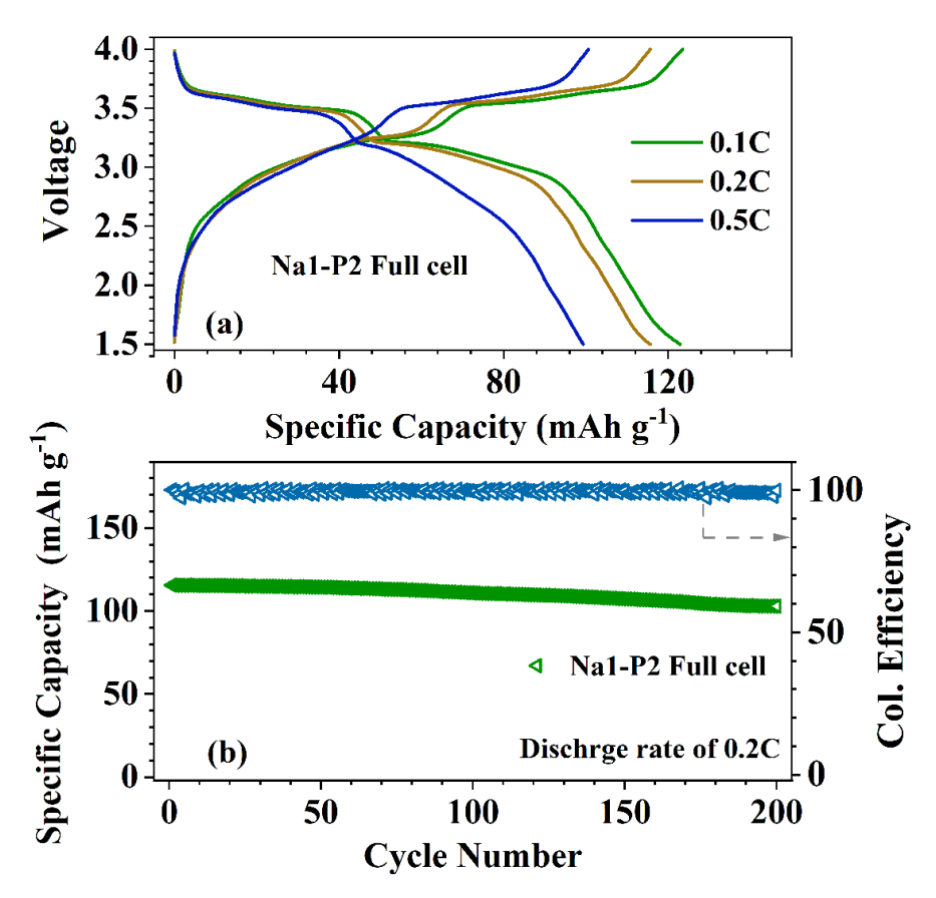


Figure 5. (a) GCD curves of Na1-P2 full cells at various C rates. (b) Cyclic performance of Na1-P2 Full cell at 0.2C along with columbic efficiency for each cycle.

Most electrochemical properties of cathode materials stem from structural changes or transformations during cycling. To explore the structural evolution of the cathode materials, operando synchrotron XRD measurements were carried out while the cells were being cycled at a constant 0.1C current. Figures S7 and 6 shows the operando SXRD patterns of Na1-P3P2 and Na1-P2 half cells at various states of charge. The XRD patterns show no visible transformations of the P3 and P2 type structures in both the cathode materials. From the onset of charging, the (002) and (003) peaks of P2 and P3 type structures in Na1-P3P2 and (002) of P2 in Na1-P2 shift to lower angles, indicating the expansion of the unit cells along the c-axis. [49-51] In contrast, the P2-type  $Na_{\frac{3}{4}}Mn_{\frac{4.5}{8}}Al_{\frac{1}{8}}Ni_{\frac{2.5}{8}}O_2$  had shown a P2 to P2' phase transition when discharged to lower voltages below 2.0 V when  $Mn^{4+/3+}$  redox couples became active, and Na concentrations increased above 0.75 in the structure. This was prevented in the biphasic P3/P2

type cathode of the same material.<sup>[18]</sup> Increasing the Na content in the same P2-type cathode material to 1.0 also prevented phase transitions in the P2-type structure, especially at low voltages.

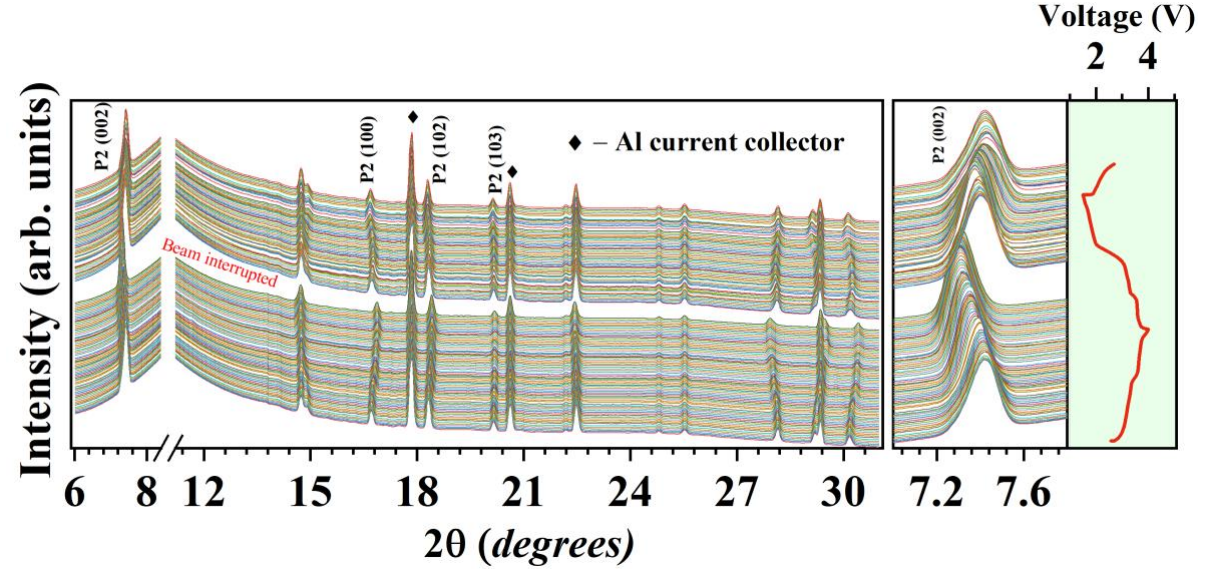


Figure 6. Operando Synchrotron XRD patterns of Na1-P2 half-cell obtained at 0.1C.

Lebail fitting was employed to analyze the operando XRD patterns of both cathodes (Figure S8-S9). The analysis confirmed the absence of any phase transformations in P3 and P2 type structures in both materials. Figure S10 and Figure 7 display the variation in the *c* parameter and unit cell volume obtained from the Lebail fitting of both the cathode materials. The changes in the *c* parameter follow an expected trend. The maximum *c* parameter is obtained at the end of changing, and the minimum is observed at the end of the discharge. In contrast, the changes in unit cell volume follow the opposite trend due to the contraction of the unit cells along the *a* and *b* axis during charging and expansion on discharging. The fluctuation in cell volume in P2 type structures in Na1-P3P2 and Na1-P2 structures was calculated to be about 0.86% and 0.78%, respectively. The relatively low variation in unit cell volume and the absence of transformations in both the cathode materials led to their high-rate performance and excellent cyclic stability.

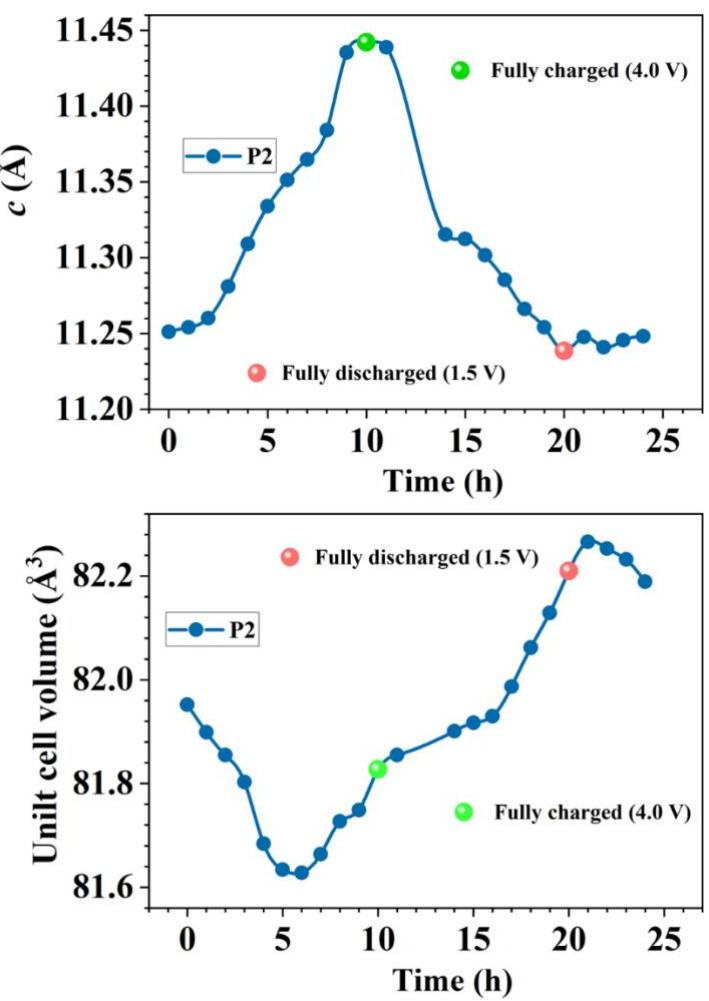


Figure 7. Variation in the c and unit cell volume parameter of P2 in Na1-P2 cathode during cycling.

## Conclusion

A high Na-containing NaMn $_{\frac{4.5}{8}}$ Al $_{\frac{1}{8}}$ Ni $_{\frac{2.5}{8}}$ O $_{2}$ layered oxide cathode material was prepared through a conventional sol-gel method. The material was prepared in 3 different phase configurations: monophasic P3, monophasic P2 (with  $\sim$  9%O3 phase), and a biphasic P3/P2 with equal proportions of P3 and P2. The phase purity and crystallographic parameters were analyzed using XRD data, which also confirmed the presence of a minor O3 phase in both the biphasic and monophasic P2 samples. The electrochemical performance parameters of the cathode materials were investigated in a half-cell configuration between 1.5 V and 4.0 V. During electrochemical testing, both the biphasic and the monophasic P2 type compound demonstrated

exceptional rate performance exhibiting specific capacities as high as 102 mAh g<sup>-1</sup> and 87 mAh g<sup>-1</sup> respectively at 6C. These materials also showed excellent cyclic stability by retaining 73% and 80% of their specific capacities after 300 cycles at 1C. Further, a full cell fabricated with the monophasic P2-type cathode material exhibited a specific capacity of 123 mAh g<sup>-1</sup> at 0.1C and retained 90% of its initial specific capacity at 0.2C after 200 cycles. The excellent cyclic stability of the monophasic P2 and biphasic cathode material was attributed to the absence of structural transformations in these materials, as corroborated by operando synchrotron XRD data. Furthermore, the unit cell volume expansion of the P2 structure in both materials was only around 0.78%.

# Acknowledgments

SK thanks the Ministry of Education (MoE) and Science and Engineering Research Board (SERB), Government of India, for the financial support under grant number MoE-STARS/STARS-2/2023-0365 and CRG/2021/005548, respectively.

## **Declaration of Interest**

The authors declare no conflict of interest

## References

- [1] J.-M. Tarascon, *Joule* **2020**, 4, 1616.
- [2] Y. E. Durmus, H. Zhang, F. Baakes, G. Desmaizieres, H. Hayun, L. Yang, M. Kolek, V. Küpers, J. Janek, D. Mandler, S. Passerini, Y. Ein-Eli, *Adv. Energy Mater.* **2020**, 10, 2000089.
- [3] J. Darga, J. Lamb, A. Manthiram, *Energy Technol.* **2020**, 8, 2000723.
- [4] R. J. Clément, P. G. Bruce, C. P. Grey, J. Electrochem. Soc. 2015, 162, A2589.
- [5] R. Usiskin, Y. Lu, J. Popovic, M. Law, P. Balaya, Y.-S. Hu, J. Maier, *Nature Rev. Mater.* **2021**, 6, 1020.
- [6] E. Goikolea, V. Palomares, S. Wang, I. R. de Larramendi, X. Guo, G. Wang, T. Rojo, *Adv. Energy Mater.* **2020**, 10, 2002055.
- [7] Y. Tian, G. Zeng, A. Rutt, T. Shi, H. Kim, J. Wang, J. Koettgen, Y. Sun, B. Ouyang, T. Chen, Z. Lun, Z. Rong, K. Persson, G. Ceder, *Chem. Rev.* **2021**, 121, 1623.
- [8] V. Palomares, P. Serras, I. Villaluenga, K. B. Hueso, J. Carretero-González, T. Rojo, *Energy Environ. Sci.* **2012**, 5, 5884.
- [9] X. Xiang, K. Zhang, J. Chen, Adv. Mater. 2015, 27, 5343.
- [10] T. Liu, B. Wang, X. Gu, L. Wang, M. Ling, G. Liu, D. Wang, S. Zhang, *Nano Energy* **2016**, 30, 756.
- [11] P.-F. Wang, Y. You, Y.-X. Yin, Y.-S. Wang, L.-J. Wan, L. Gu, Y.-G. Guo, *Angew. Chem. Int. Ed.* **2016**, 55, 7445.
- [12] Y. Li, Z. Yang, S. Xu, L. Mu, L. Gu, Y.-S. Hu, H. Li, L. Chen, *Adv. Sci. (Weinh)* **2015**, 2, 1500031.
- [13] L. Xian, M. Li, D. Qiu, C. Qiu, C. Yue, F. Wang, R. Yang, *J. Alloys Compd.* **2022**, 905, 163965.
- [14] T. Risthaus, L. Chen, J. Wang, J. Li, D. Zhou, L. Zhang, D. Ning, X. Cao, X. Zhang, G. Schumacher, M. Winter, E. Paillard, J. Li, *Chem. Mater.* **2019**, 31, 5376.
- [15] H. N. Vasavan, M. Badole, S. Dwivedi, D. Kumar, P. Kumar, S. Kumar, *Chem. Eng. J.* **2022**, 448, 137662.
- [16] H. N. Vasavan, M. Badole, S. Dwivedi, S. Kumar, *Ceram. Int.* **2022**, 48, 28986.
- [17] H. N. Vasavan, M. Badole, S. Saxena, A. K. Das, S. Deswal, P. Kumar, S. Kumar, *ACS Appl. Energy Mater.* **2023**, 6, 2440.
- [18] H. N. Vasavan, M. Badole, S. Saxena, V. Srihari, A. K. Das, P. Gami, N. Dagar, S. Deswal, P. Kumar, H. K. Poswal, S. Kumar, *J. Energy Chem.* **2024**, 96, 206.
- [19] H. N. Vasavan, M. Badole, S. Saxena, V. Srihari, A. K. Das, P. Gami, N. Dagar, S. Deswal, P. Kumar, H. K. Poswal, S. Kumar, *Electrochim. Acta* **2024**, 494, 144457.
- [20] H. N. Vasavan, M. Badole, S. Saxena, V. Srihari, A. K. Das, P. Gami, S. Deswal, P. Kumar, S. Kumar, *Mater. Today Energy.* **2023**, 37, 101380.
- [21] H. N. Vasavan, M. Badole, S. Saxena, V. Srihari, A. K. Das, P. Gami, S. Deswal, P. Kumar, S. Kumar, *J. Energy Storage* **2023**, 74, 109428.
- [22] Q. Liu, Z. Hu, W. Li, C. Zou, H. Jin, S. Wang, S. Chou, S.-X. Dou, *Energy Environ. Sci.* **2021**, 14, 158.
- [23] Y.-N. Zhou, P.-F. Wang, Y.-B. Niu, Q. Li, X. Yu, Y.-X. Yin, S. Xu, Y.-G. Guo, *Nano Energy* **2019**, 55, 143.
- [24] B. Peng, G. Wan, N. Ahmad, L. Yu, X. Ma, G. Zhang, *Adv. Energy Mater.* **2023**, 13, 2300334.
- [25] E. Gabriel, C. Ma, K. Graff, A. Conrado, D. Hou, H. Xiong, eScience 2023, 3, 100139.

- [26] C. Zhao, Z. Yao, Q. Wang, H. Li, J. Wang, M. Liu, S. Ganapathy, Y. Lu, J. Cabana, B. Li, X. Bai, A. Aspuru-Guzik, M. Wagemaker, L. Chen, Y.-S. Hu, *J. Am. Chem. Soc.* **2020**, 142, 5742.
- [27] S. Saxena, M. Badole, H. N. Vasavan, V. Srihari, A. K. Das, P. Gami, S. Deswal, P. Kumar, S. Kumar, *Chem. Eng. J.* **2024**, 485, 149921.
- [28] S. Saxena, H. N. Vasavan, M. Badole, A. K. Das, S. Deswal, P. Kumar, S. Kumar, *J. Energy Storage* **2023**, 64, 107242.
- [29] X. Liang, T.-Y. Yu, H.-H. Ryu, Y.-K. Sun, Energy Storage Mater. 2022, 47, 515.
- [30] L. Yu, Y.-X. Chang, M. Liu, Y.-H. Feng, D. Si, X. Zhu, X.-Z. Wang, P.-F. Wang, S. Xu, *ACS Appl. Mater. Interfaces* **2023**, 15, 23236.
- [31] X. Li, X. Shen, J. Zhao, Y. Yang, Q. Zhang, F. Ding, M. Han, C. Xu, C. Yang, H. Liu, Y.-S. Hu, *ACS Appl. Mater. Interfaces* **2021**, 13, 33015.
- [32] R. Li, Y. Liu, Z. Wang, J. Li, *Electrochim. Acta* **2019**, 318, 14.
- [33] B. Peng, Y. Chen, L. Zhao, S. Zeng, G. Wan, F. Wang, X. Zhang, W. Wang, G. Zhang, *Energy Storage Mater.* **2023**, 56, 631.
- [34] L. Yu, X. He, B. Peng, F. Wang, N. Ahmad, Y. Shen, X. Ma, Z. Tao, J. Liang, Z. Jiang,
   Z. Diao, B. He, Y. Xie, B. Qing, C. Wang, Y. Wang, G. Zhang, Adv. Funct. Mater.
   2024, 34, 2406771.
- [35] S. Saxena, M. Badole, H. N. Vasavan, V. Srihari, A. K. Das, P. Gami, N. Dagar, S. Deswal, P. Kumar, H. K. Poswal, S. Kumar, *Energy & Fuels* **2024**, 38, 12140.
- [36] A. Coelho, J. Appl. Crystallogr. 2018, 51, 210.
- [37] X. Liu, W. Zuo, B. Zheng, Y. Xiang, K. Zhou, Z. Xiao, P. Shan, J. Shi, Q. Li, G. Zhong, R. Fu, Y. Yang, *Angew. Chem. Int. Ed.* 2019, 58, 18086.
- [38] V. Pamidi, S. Trivedi, S. Behara, M. Fichtner, M. A. Reddy, *iScience* **2022**, 25, 104205.
- [39] Z. Zhang, R. Wang, J. Zeng, K. Shi, C. Zhu, X. Yan, *Adv. Funct. Mater.* **2021**, 31, 2106047.
- [40] W. Kang, D. Y. W. Yu, P.-K. Lee, Z. Zhang, H. Bian, W. Li, T.-W. Ng, W. Zhang, C.-S. Lee, *ACS Appl. Mater. Interfaces* **2016**, 8, 31661.
- [41] J. F. Moulder, J. Chastain, *Handbook of X-ray Photoelectron Spectroscopy: A Reference Book of Standard Spectra for Identification and Interpretation of XPS Data*, Physical Electronics Division, Perkin-Elmer Corporation, **1992.**
- [42] S. Hüfner, *Photoelectron spectroscopy: principles and applications*, Springer Science & Business Media, **2013.**
- [43] X.-H. Zhang, W.-L. Pang, F. Wan, J.-Z. Guo, H.-Y. Lü, J.-Y. Li, Y.-M. Xing, J.-P. Zhang, X.-L. Wu, *ACS Appl. Mater. Interfaces* **2016**, 8, 20650.
- [44] P. Manikandan, D. Ramasubramonian, M. M. Shaijumon, *Electrochim. Acta* **2016**, 206, 199.
- [45] X. Wu, J. Guo, D. Wang, G. Zhong, M. J. McDonald, Y. Yang, *J. Power Sources* **2015**, 281, 18.
- [46] H. Liu, X. Gao, J. Chen, J. Gao, S. Yin, S. Zhang, L. Yang, S. Fang, Y. Mei, X. Xiao, L. Chen, W. Deng, F. Li, G. Zou, H. Hou, X. Ji, *J. Power Sources* **2021**, 508, 230324.
- [47] Y. Xie, H. Wang, G. Xu, J. Wang, H. Sheng, Z. Chen, Y. Ren, C.-J. Sun, J. Wen, J. Wang, D. J. Miller, J. Lu, K. Amine, Z.-F. Ma, *Adv. Energy Mater.* **2016**, 6, 1601306.
- [48] P.-F. Wang, Y.-J. Guo, H. Duan, T.-T. Zuo, E. Hu, K. Attenkofer, H. Li, X. S. Zhao, Y.-X. Yin, X. Yu, Y.-G. Guo, *ACS Energy Lett.* **2017**, 2, 2715.
- [49] X.-M. Lin, X.-T. Yang, H.-N. Chen, Y.-L. Deng, W.-H. Chen, J.-C. Dong, Y.-M. Wei, J.-F. Li, *J. Energy Chem.* **2023**, 76, 146.
- [50] Z. Lu, J. R. Dahn, J. Electrochem. Soc. 2001, 148, A1225.
- [51] Y.-N. Zhou, Z. Xiao, D. Han, S. Wang, J. Chen, W. Tang, M. Yang, L. Shao, C. Shu, W. Hua, D. Zhou, Y. Wu, *J. Mater. Chem. A* **2023**, 11, 2618.

## [Supporting Information]

# Elevating the Concentration of Na ions to 1 in P2 Type Layered Oxide Cathodes

Hari Narayanan Vasavan<sup>a</sup>\*, Samriddhi Saxena<sup>a</sup>, Velaga Srihari<sup>b</sup>, Asish Kumar Das<sup>a</sup>, Pratiksha Gami<sup>a</sup>, Neha Dagar<sup>a</sup>, Sonia Deswal<sup>c</sup>, Pradeep Kumar<sup>c</sup>, Himanshu Kumar Poswal<sup>b</sup>, and Sunil Kumar<sup>a,\*\*</sup>

<sup>a</sup> Department of Metallurgical Engineering and Materials Science, Indian Institute of Technology Indore, Simrol, 453552, India.

<sup>b</sup> High Pressure & Synchrotron Radiation Physics Division, Bhabha Atomic Research Centre, 400085 Mumbai, India

<sup>c</sup> School of Physical Sciences, Indian Institute of Technology Mandi, Himachal Pradesh, 175005, India

\* mtphd2206105002@iiti.ac.in

\*\* Corresponding Author: sunil@iiti.ac.in

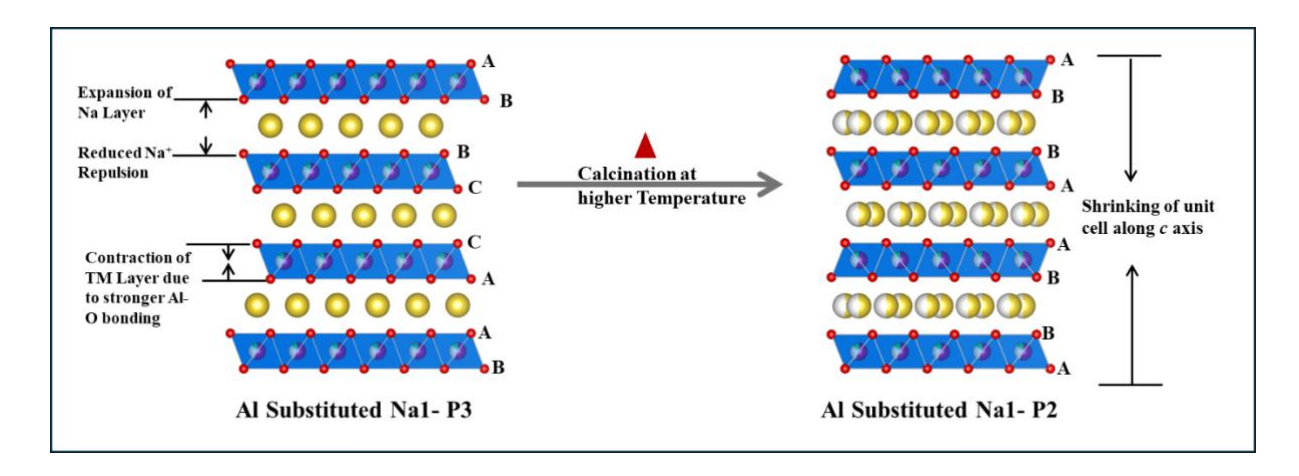


Figure S1. Schematic representing the conversion of Na1-P3 to Na1-P2 at higher calcination temperature.

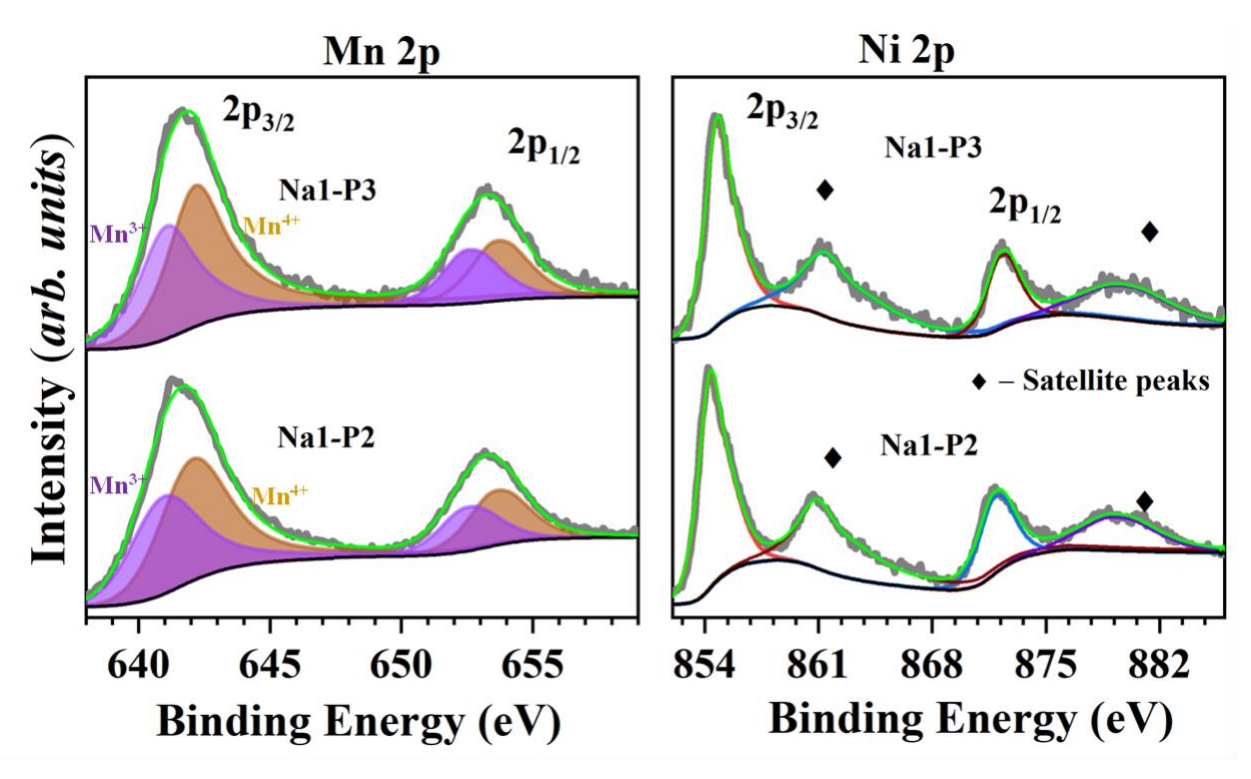


Figure S2. Mn 2p and Ni 2p XPS plots of Na1-P3 and Na1-P2 samples.

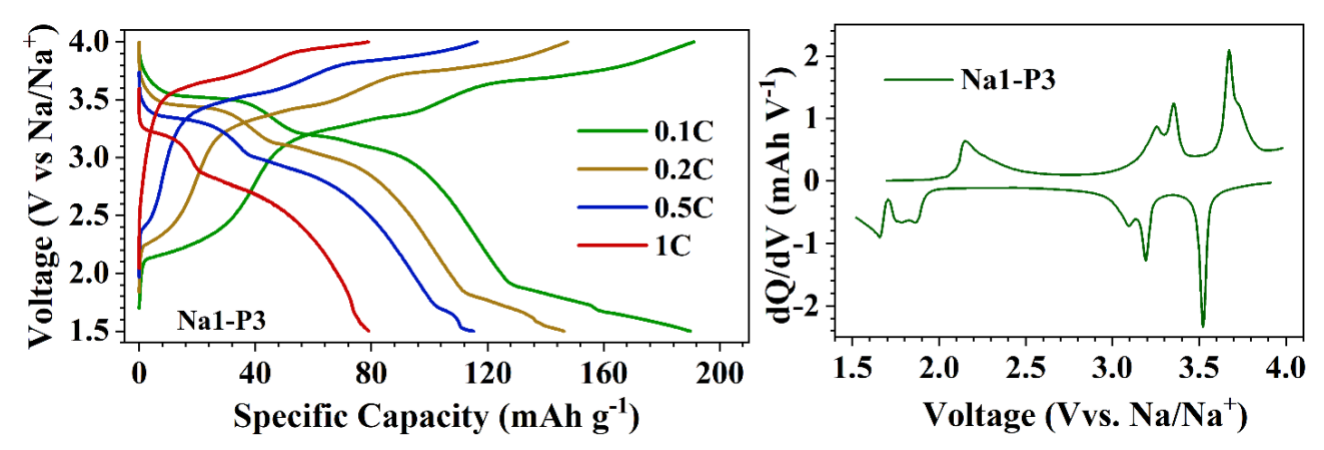


Figure S3. GCD curves of Na1-P3 cathode material at different C rates along with its dQ/dV vs.

voltage plots at 0.1C.

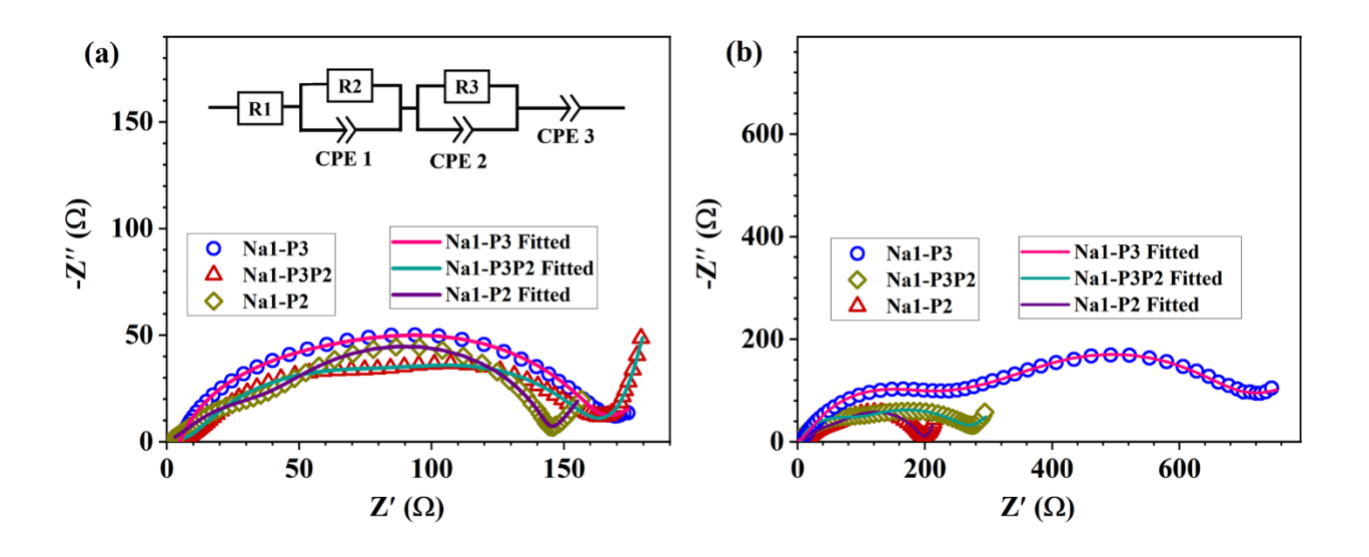


Figure S4. (a) Nyquist plots of Na1-P3, Na1-P3P2, and Na1-P2 half cells (a) before and (b) after 300 cycles. Figure inset shows the equivalent circuit used to fit the impedance data.

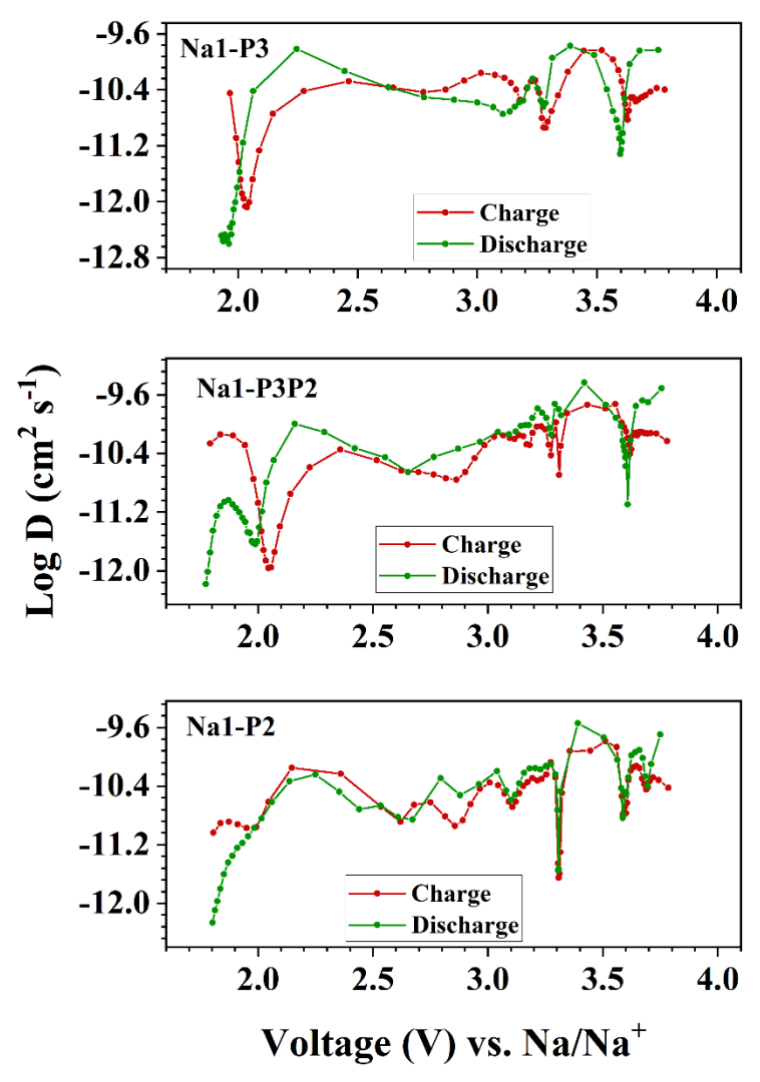


Figure S5. Variation of diffusion coefficients of Na1-P3, Na1-P3P2, and Na1-P2 cathodes during a charge/discharge cycle.

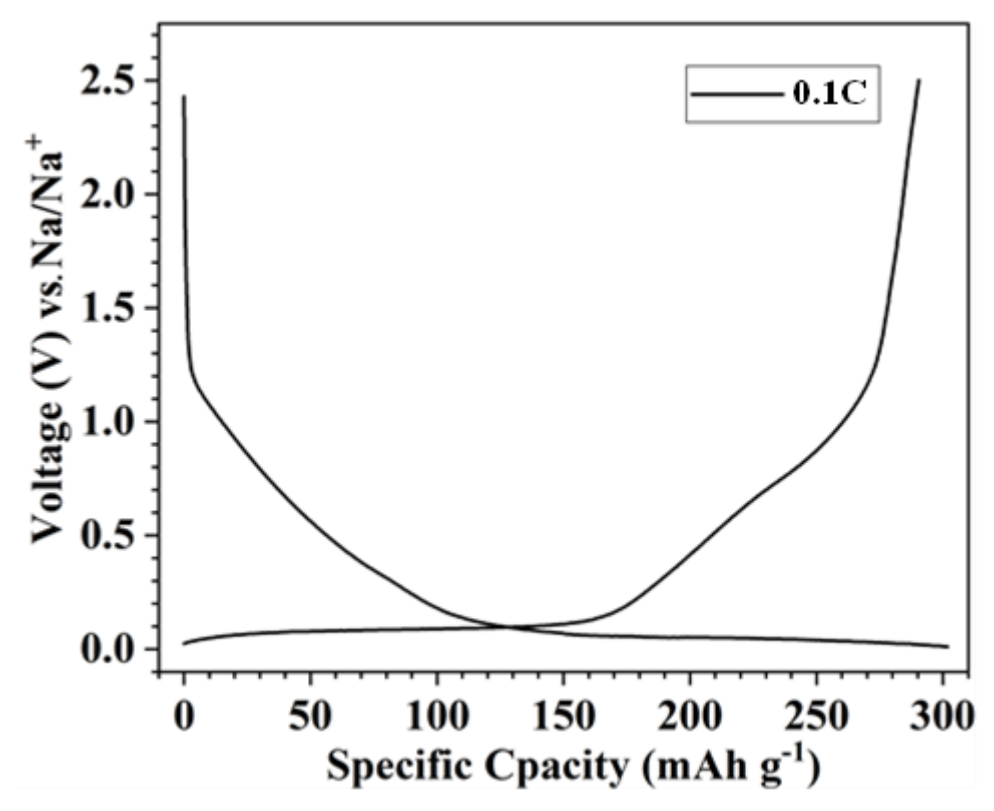


Figure S6. GCD curve of a hard carbon half cell.

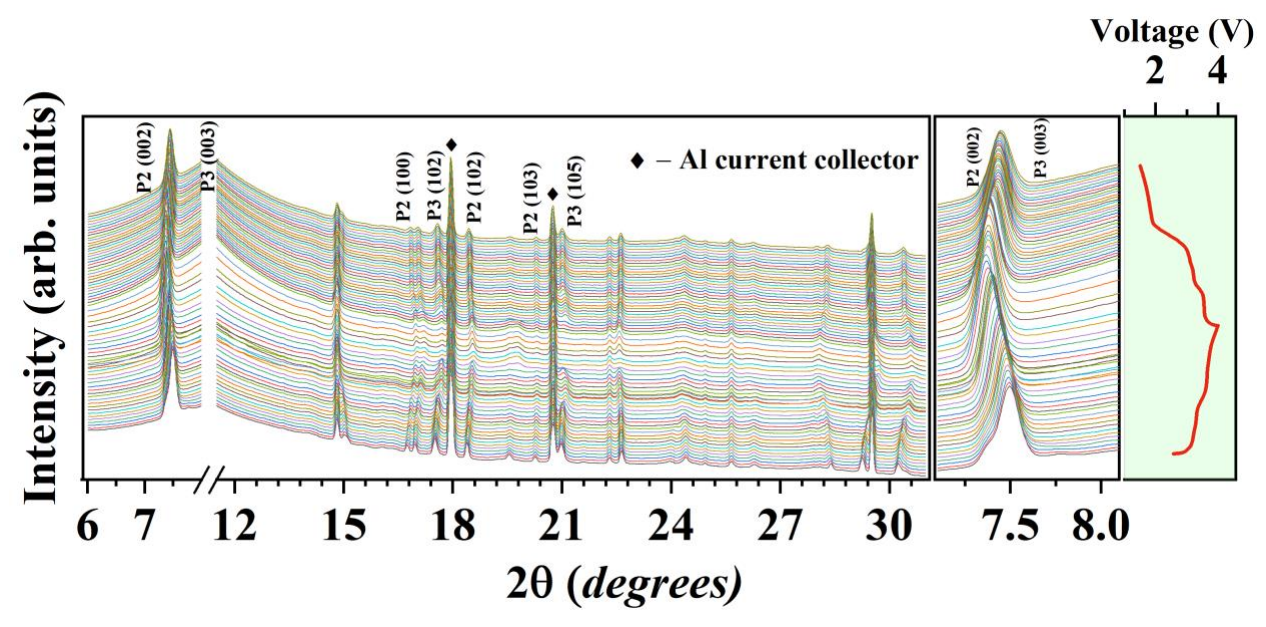


Figure S7. Operando Synchrotron XRD patterns of Na1-P3P2 obtained at 0.1C.

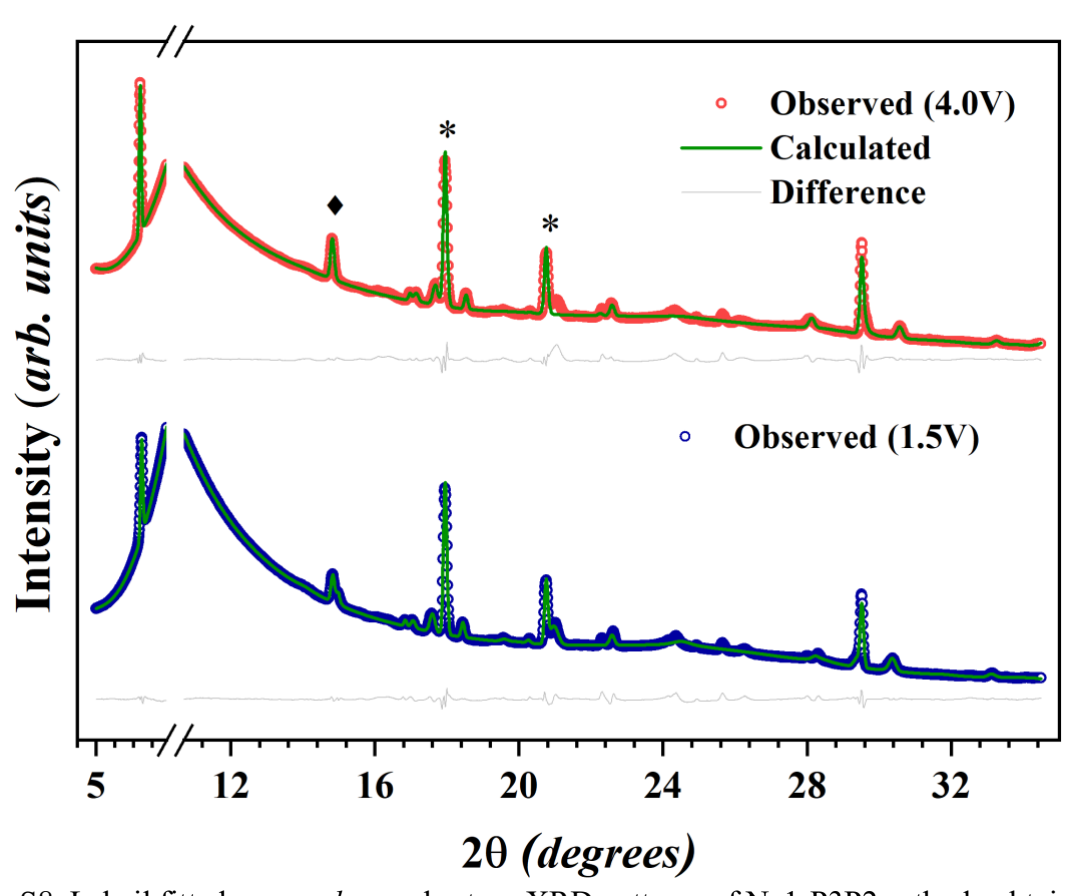


Figure S8. Lebail fitted *operando* synchrotron XRD patterns of Na1-P3P2 cathode obtained at fully charged (4.0 V) and fully discharged (1.5 V) states.

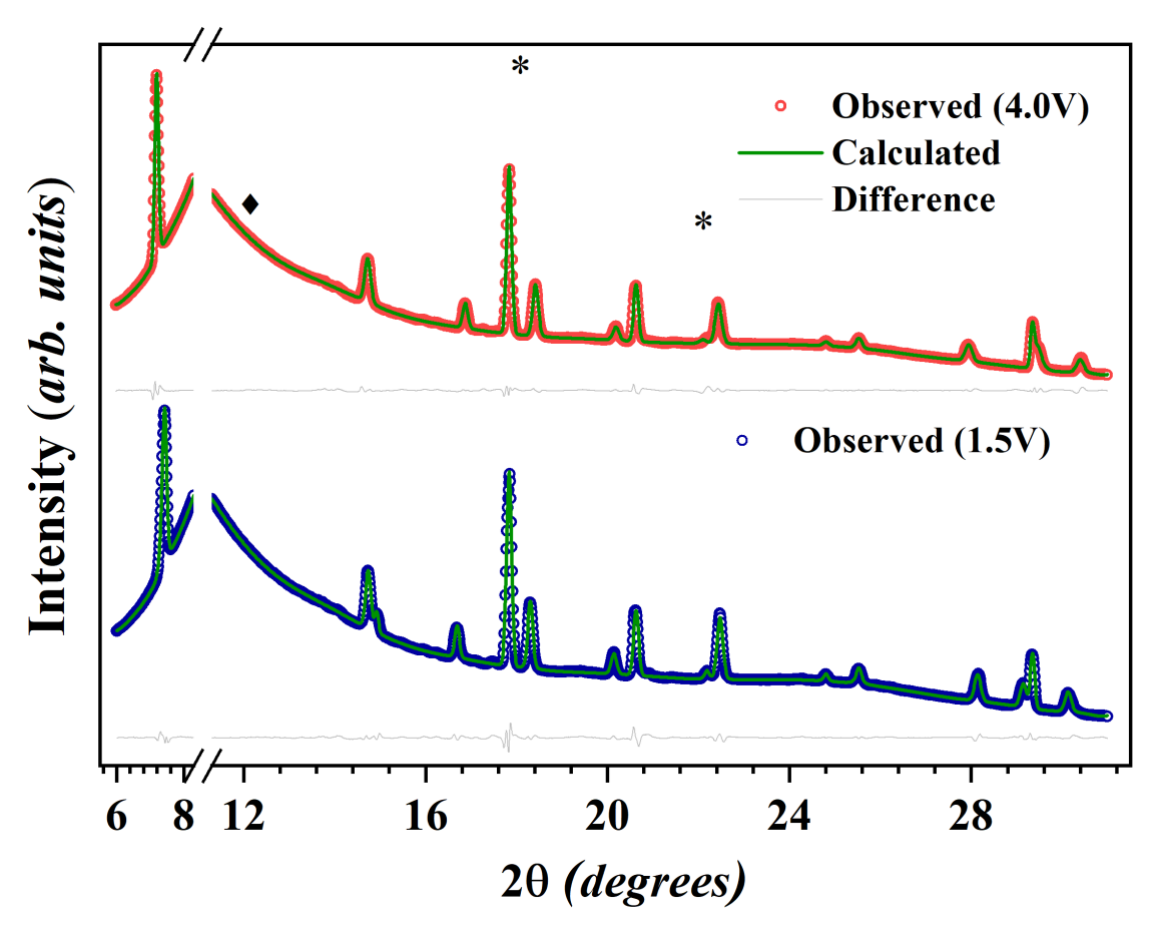


Figure S9. Lebail fitted *operando* synchrotron XRD patterns of Na1-P2 cathode obtained at fully charged (4.0 V) and fully discharged (1.5 V) states.

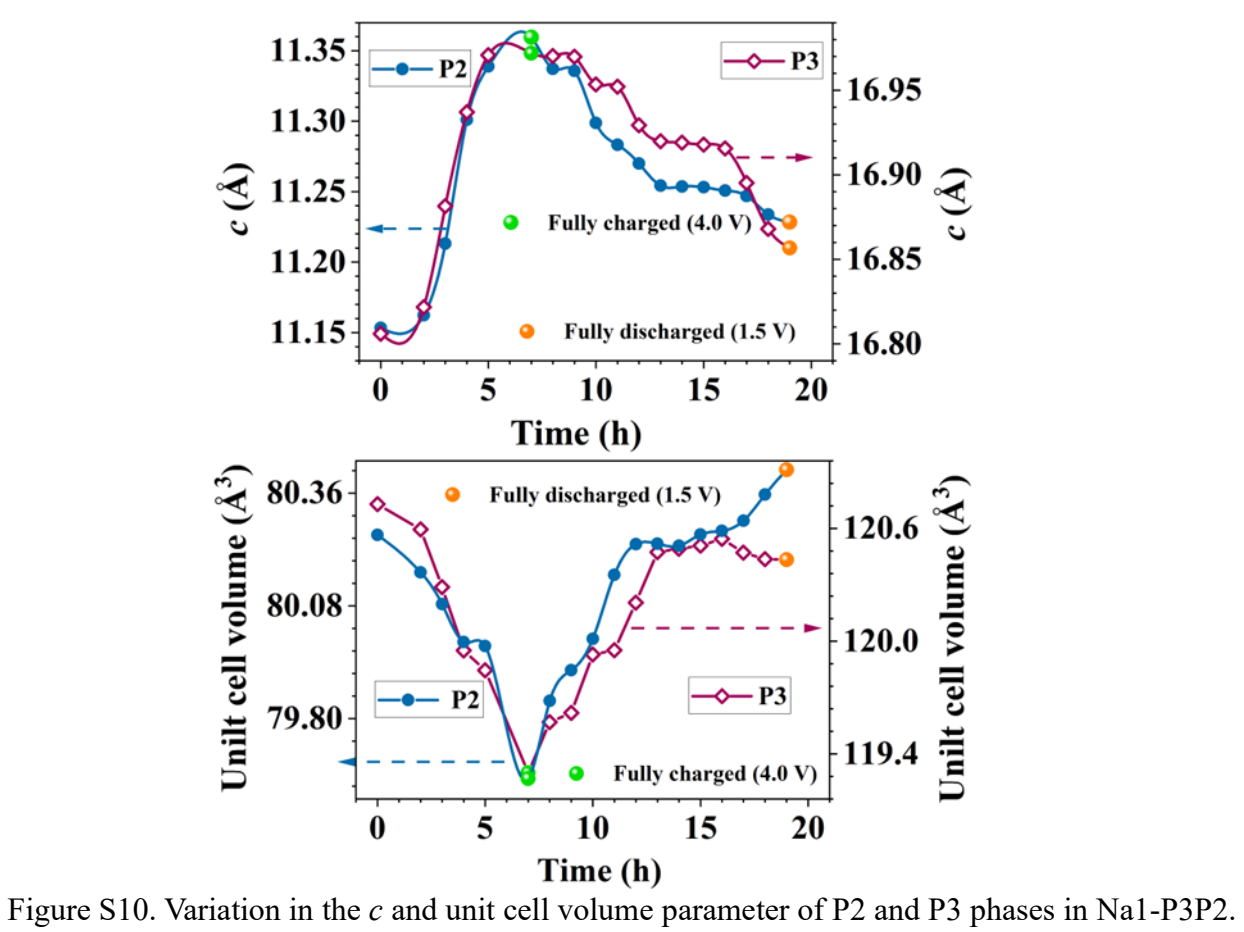


Table S1. The chemical compositions of the as-prepared samples were measured by inductively coupled plasma atomic emission spectroscopy (ICP-AES).

Cample	Calculated composition  Na/ Mn/ Ni/ Al		
Sample			
Na1-P3	0.997/0.562/0.312/0.123		
Na1-P3P2	0.993/0.562/0.312/0.122		
Na1-P2	0.99/0.562/0.311/0.123		